Acta Crystallographica Section D
Biological Crystallography
ISSN 0907-4449

Three-dimensional structure of homodimeric cholesterol esterase–ligand complex at 1.4 Å resolution

Vladimir Pletnev,[a,b] Anthony Addlagatta,[b] Zdzislaw Wawrzak[c] and William Duax[b,d]*

[a]Institute of Bioorganic Chemistry, Russian Academy of Science, Moscow, Russia, [b]Hauptman–Woodward Medical Research Institute, Buffalo, New York, USA, [c]Northwestern University, Argonne, IL, USA, and [d]SUNY at Buffalo, Buffalo, NY 14214, USA

Correspondence e-mail: duax@hwi.buffalo.edu

Received 20 June 2002
Accepted 14 October 2002

PDB Reference: cholesterol esterase–ligand complex, 1llf, r1llfsf.

The three-dimensional structure of a *Candida cylindracea* cholesterol esterase (ChE) homodimer (534 × 2 amino acids) in complex with a ligand of proposed formula $C_{23}H_{48}O_2$ has been determined at 1.4 Å resolution in space group *P*1 using synchrotron low-temperature data. The structure refined to R = 0.136 and R_{free} = 0.169 and has revealed new stereochemical details in addition to those detected for the apo- and holo-forms at 1.9 and 2.0 Å resolution, respectively [Ghosh *et al.* (1995), *Structure*, **3**, 279–288]. The cholesterol esterase structure is a dimer with four spatially separated interfacial contact areas and two symmetry-related pairs of openings to an internal intradimer cavity. Hydrophobic active-site gorges in each subunit face each other across a central interfacial cavity. The ChE subunits have carbohydrate chains attached to their Asn314 and Asn351 residues, with two ordered *N*-acetyl-D-glucosoamine moieties visible at each site. The side chains of 14 residues have two alternative conformations with occupancy values of 0.5 ± 0.2. For each subunit the electron density in the enzyme active-site gorge is well modeled by a C_{23}-chain fatty acid.

1. Introduction

Cholesterol esterase (ChE; EC 3.1.1.13) from the fungus *Candida cylindracea* (and the closely related *Psudomonas fluoresence*) is a glycoprotein that belongs to the lipase/esterase family (Cygler & Schrag, 1999). ChE hydrolyzes many fatty-acid esters of cholesterol. The rate of hydrolysis is greater for long-chain than for short-chain fatty-acid esters and is greater for unsaturated than for saturated fatty-acid esters. Relative rates for hydrolysis of cholestrol esters by the enzyme are as follows: linoleate (18 C atoms/two double bonds), 100; elaidate (18/1), 78; palmitate (16/0), 65; oleate (18/1), 55; stearate (18/0), 22; caprinate (10/0), 12; caproate (6/0), 10; propionate (3/0), 7; acetate (2/0), 2 (Bergmeyer *et al.*, 1983; Uwajima & Terada, 1975; Roeschlau *et al.*, 1974). The best substrate which ChE reversibly hydrolyzes is cholesteryl linoleate, the ester of the unsaturated fatty acid. Cholesteryl linoleate and cholesteryl oleate are the major components of arterial plaque (Small, 1989).

We previously published the structures of free and linoleate-bound forms of *C. cylindracea* cholesterol esterase based on 1.9 and 2.0 Å resolution data collected at ambient temperature (Ghosh *et al.*, 1995). In this paper, we present new structural details revealed by an X-ray study of the enzyme in complex with a C_{23}-chain fatty acid of proposed formula $C_{23}H_{48}O_2$ (FA23) using low-temperature 1.4 Å resolution data.

© 2003 International Union of Crystallography
Printed in Denmark – all rights reserved

Table 1
Crystallographic data.

Values in parentheses are for the last resolution shell (1.5–1.4 Å).

Space group	*P*1
Unit-cell parameters (Å, °)	a = 58.461, b = 58.477, c = 89.515, α = 92.708, β = 97.476, γ = 109.380
Monomers per cell	2
Estimated solvent content (%)	42
Temperature (K)	100
Wavelength (Å)	1.0
Resolution range (Å)	30–1.4
Total reflections measured	1424531
Unique reflections observed	206525
$R_{\rm merge}$	0.087 (0.178)
Completeness (%)	90.2 (88.0)
$I < 2\sigma(I)$ (%)	2.6 (7.0)

2. Materials and methods

2.1. Crystallization and data collection

Commercially available *C. cylindracea* cholesterol esterase (ChE; from Roche Molecular Biochemicals) was further purified according to published procedures (Kaiser *et al.*, 1994), with separation of two fractions corresponding to monomeric and dimeric forms. Crystals of ChE were grown at 293 K from the monomeric fraction by the hanging-drop technique as described previously (Ghosh *et al.*, 1991; Kaiser *et al.*, 1994). The monomeric form was incubated with the polymer detergent Thesit, $C_{12}H_{25}O(CH_2CH_2O)_n$ (Sigma–Aldrich); droplets of enzyme solution were stabilized with PEG 3350 (Sigma) and 50 m*M* phosphate buffer pH 7.3 and set up for vapour diffusion against sealed wells containing reservoirs of 21% PEG solution in the same buffer. The Thesit detergent was found to be an essential component of the crystallization media for the monomeric fraction of the enzyme (in contrast to the dimeric fraction). Crystals of optimal size grew within two weeks.

Low-temperature X-ray diffraction data to 1.4 Å resolution were collected at the Argonne Synchrotron Source and were processed with the software *DENZO* (Otwinowski & Minor, 1997). The crystallographic data are presented in Table 1.

2.2. Crystallographic refinement

The structure was determined by the molecular-replacement technique with the program *AMoRe* (Navaza, 1994), using the 2 Å resolution dimer model (Ghosh *et al.*, 1995) as a search probe. The crystallographic refinement was initially performed using *CNS* (Brünger *et al.*, 1998) and was completed using the *SHELX*97 package (Sheldrick, 1997). The resolution was gradually extended to 1.4 Å. Anisotropic treatment of the non-H atom thermal motion was introduced at the final stage of refinement and resulted in improvement of the $R_{\rm free}$ value by 2.6%. The stereochemically ideal positions of the H atoms were calculated after each of the last three cycles. The refinement process included manual adjustment of the model in the electron density using the program *CHAIN* (Sack, 1988). A summary of the refinement results is presented in Table 2.

Table 2
Refinement statistics.

Highest resolution (Å)	1.4
Non-H atoms in model	
Protein† (2 × 534 residues)	8074
Sugar (2 × 4 NAGs)	112
Ligand (2 × 1 FA23)	50
Water	1078
H atoms in model	8064
No. of protein side chains with two conformations (occ = 0.5 ± 0.2)	14
$R_{\rm cryst}$ (95% data, $F \geq 0$)	0.136
$R_{\rm free}$ (5% data, $F \geq 0$)	0.169
Goodness of fit	3.70
Restrained goodness of fit	2.87
Average *B* factor (Å^2)	
Protein	14.18
Ligand	23.69
Water	25.16
R.m.s.d. from ideal values	
Bond distance (Å)	0.011
Bond angle (°)	2.03
Planarity (°)	1.54
Dihedral angle (°)	24.44
Ramachandran plot statistics (%) [for 892 non-Gly/Pro residues]	
Most favoured and other allowed regions	99.3

† In the definition adopted, the residue numbering for the first subunit of the ChE dimer runs from 1 to 534 and for the second subunit from 1001 to 1534.

Analysis of the molecular geometry was performed with the *CNS* (Brünger *et al.*, 1998), *CCP*4 (Collaborative Computational Project, Number 4, 1994) and *PROCHECK* (Laskowski *et al.*, 1993) packages. The illustrations were produced with the *SETOR* (Evans, 1993) and *LIGPLOT*/*HBPLUS* (Wallace *et al.*, 1995; McDonald & Thornton, 1994) programs.

3. Results and discussion

3.1. Overall structure and interfacial association

The subunits in the cholesterol esterase (ChE) structure are related by a non-crystallographic twofold pseudosymmetry axis (Fig. 1) with an r.m.s. deviation of <0.1 Å for all 534 C$^\alpha$ atoms. Each subunit has a single α/β-type domain, with a 13-stranded β-sheet at the core surrounded by 16 α-helices.

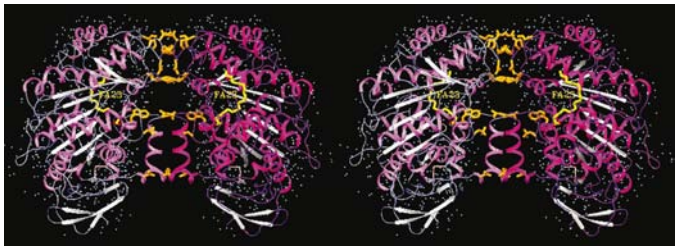

Figure 1
Stereoview of the ChE dimer structure with the side chains in the four contact areas shown in brown, two fatty-acid ligands FA23 in the active-site gorge shown in yellow with red O atoms and the water molecules represented by blue spots. The α-helices and the β-strands are shown in magenta and white, respectively. The subunits are related by a non-crystallographic twofold symmetry axis (ribbon presentation). Figure produced using *SETOR* (Evans, 1993).

The overall structural features and the interfacial association of the two subunits of the ChE complex with the proposed fatty-acid ligand FA23 at 1.4 Å resolution are nearly identical to those observed in the ChE linoleate-bound form at 2 Å resolution (Ghosh *et al.*, 1995). The r.m.s. deviation between the structure based upon the two data sets is 0.68 Å for all 1068 C^{α} atoms. Atomic details of the flexible 'flap' region 65–91 (1065–1091) were well resolved in the higher resolution data. This flap, including two α-helices 73–83 (1073–1083) and 85–90 (1085–1090) that are at a $\sim$120° angle to one another, plays an important role in dimerization.

The increased resolution of the data supports a more detailed description of the interfacial association of the two subunits than was previously presented (Ghosh *et al.*, 1995). There are four regions of significant contacts (see Fig. 1) between the subunits that form the dimer, with an internal cavity that is nearly spherical (with a radius of $\sim$7.3 Å) and almost entirely hydrophobic. The strongest stabilizing interactions are four hydrogen bonds between the symmetry-related antiparallel backbone segments 397–399 and 1397–1399 that make up the contact region at the top of the dimer as shown in Fig. 1: (Asn397)N—H···O═C(Ile1399), 2.86 Å; (Ala398)N—H···O═C(Ala1398), 3.34 Å; (Ala398)C═O···H—N(Ala1398), 3.24 Å; (Ile399)C═O···H—N(Asn1397), 2.85 Å. From beneath (from the side of the internal cavity), this hydrogen-bonded ladder is flanked by hydrophobic side chains interacting in pairs: Leu350···Pro1443, Pro443···Leu1350 and others within the cluster Ile399/Ile1399, Ile444/Ile1444 (with contact distances 3.5–3.9 Å). From the above exterior side, it is partially protected by a hydrophobic environment composed of the side chains of Ile385/Ile1385, Ile395/Ile1395, Phe396/Phe1396 and Pro401/Pro1401 from both subunits.

In the middle of a dimer there are two symmetry-related small interfacial hydrophobic clusters (with contact distances 3.6–3.9 Å) composed of the side chains of residues Leu73, Trp1455, Leu1459 and Leu1073, Trp455, Leu459, respectively. The fourth interfacial area, which is at the bottom of the structure as illustrated (distances ranging from 3.3–3.5 Å), is composed of the hydrophobic side chains of symmetry-related pairs of valines, Val86/Val1086 and Val90/Val1090.

The surface of the dimer has four sites of access to the internal cavity: two symmetry-related pairs of openings at the front and back of the molecule (Fig. 1). The openings, of approximately 7 and 9 Å diameter, are located above and below the center of the dimer, respectively. The 9 Å diameter openings are bordered by hydrophobic residues and are at entryways that allow substrate access to the catalytic site tunnels without disrupting dimer assembly.

3.2. Ligand binding

In each subunit, the primarily hydrophobic active-site tunnels are $\sim$30 Å in length and have the catalytic triad Ser209-Glu341-His449 at the opening and Tyr361, Phe362, Ser365, Phe366, Leu410 and Ile406 residues lining the bottom cup. The catalytic serine has the strained conformation (φ = +58° and ψ = −114°) typical of the analogous residue in other members of the esterase/lipase family [φ = +50° (±20°) and ψ = −135° (±20°); Bourne *et al.*, 1999; Ghosh *et al.*, 1999; Kim *et al.*, 1997; Lawson *et al.*, 1994; Grochulski *et al.*, 1994; Van Tilbeurgh *et al.*, 1993; Cygler *et al.*, 1993; Cygler & Schrag, 1999; Sussman *et al.*, 1991]. It appears that the strain is critical to the function.

Well defined electron density filled both of the symmetry-related active-site tunnels. Efforts to unequivocally identify the ligands within the tunnels by chemical and spectroscopic means have been unsuccessful. Taking into account the hydrophobic nature of the tunnel and the preference of the enzyme for substrates with long hydrocarbon chains, attempts were made to fit the density with models of $C_{12}H_{25}O(CH_2CH_2O)_3$, a terminal fragment of the Thesit detergent (THE) which was used in crystallization, and a C_{23}-chain fatty acid with proposed formula $C_{23}H_{48}O_2$ (FA23) that may have been present in the commercial sample. Both ligand models make favorable contacts with the residues lining the internal hydrophobic surface of the gorge as well as with the residues at the reactive site. The FA23 model fits the density somewhat better (Fig. 2) because it has a longer alkyl chain than the THE counterpart, which enables more favorable interaction with the hydrophobic environment of the gorge below the reactive site. Also, the clearly defined bifurcated shape of the electron density at the end of the chain beyond the reactive site is well fitted by the carboxyl group —COOH of the postulated FA23 ligand. The carboxyl group modeled in the density is stabilized by a network of hydrogen bonds involving two water molecules and the side chain of a glutamic acid residue (FA23)O1···OE1(Glu208/1208) (Fig. 3). The nearest interacting water molecules, W1 and W2, could be

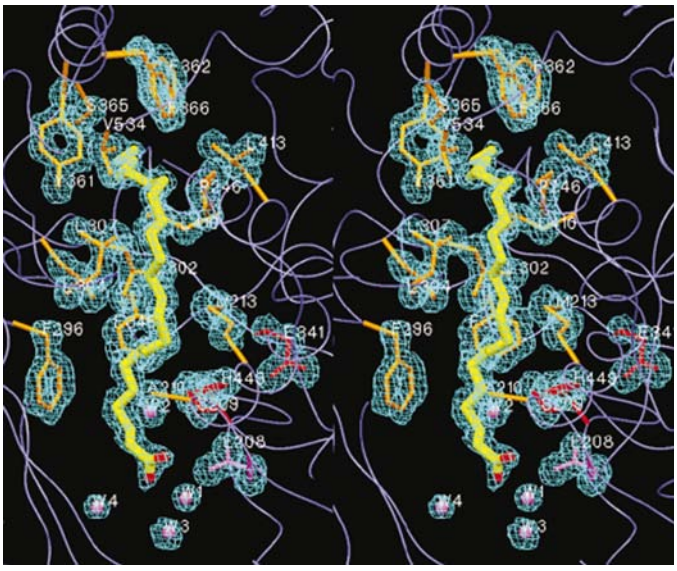

Figure 2
Stereoview of the proposed fatty-acid ligand ($C_{23}H_{48}O_2$; yellow) in the $2F_o - F_c$ electron density (blue; contoured at $1.1\sigma_\rho$) in the enzyme active site. The neighboring hydrophobic side chains are shown in brown and the catalytic triad Ser209-Glu341-His449 in red. Four water molecules (W) near the active-site exit are shown as magenta spheres. Figure produced using *SETOR* (Evans, 1993).

alternative proton sources. W2, which mediates the interactions between the ligand and the enzyme, can form up to four hydrogen bonds with tetrahedral geometry. The terminal atom of the ligand, C23, extends to the very bottom of the binding tunnel. No *cis* configuration indicative of a C=C double bond in the ligand was detected. The COOH group of the modeled FA23 ligand is ~4.0 Å away from the optimal reactive position of the cleaved ester bond in the enzyme catalytic triad area. It extends beyond the reactive site into the intradimer internal cavity.

It is of interest to compare the ligand-binding structural features of the ChE–FA23 complex with those of the linoleate-bound form (Ghosh *et al.*, 1995) and the functionally related *C. rugosa* lipase complexes with the covalently bound inhibitors menthyl hexyl phosphonate (MPC; $C_{16}H_{32}PO_2$), dodecanesulfonate (DSC; $C_{12}H_{26}SO_2$) and hexadecanesulfonate (HDS; $C_{16}H_{34}SO_2$) (Grochulski *et al.*, 1994). Pairwise least-squares superposition of the compared subunits for all 534 C^{α} atoms reveals almost identical backbone tracing for all enzyme structures (with r.m.s. deviations of 0.29, 0.38, 0.37, 0.36 Å, respectively) including the active-site-binding tunnel area. For both ChE complexes the positions of the enzyme side chains lining the tunnel are practically the same. However, the presence of two *cis* C=C double bonds in the linoleate ligand, in contrast to the all *trans* and *gauche* C—C single bonds in the saturated FA23 counterpart, results in local conformational differences along the same general ligand path below the enzyme reactive site (Fig. 4). The *C. rugosa* lipase inhibitors, MPC, DSC and HDS, have six-, 12- and 16-membered saturated alkyl chains attached to their P or S atom. The overlapping parts of these chains show high conformational similarity among themselves as well as with an analogous fragment of the FA23 model. In the ChE and lipase complexes with FA23 and HDS, involving the longest alkyl chains, the corresponding central ten-atom fragments C11–C20 and C4–C13 of both ligands occupy essentially the same position (Fig. 4). Significant conformational differences occur at either end of this common fragment, in the position of the three C-atom termini at the bottom of the tunnel and, more essentially, at the reactive site, where the binding-state

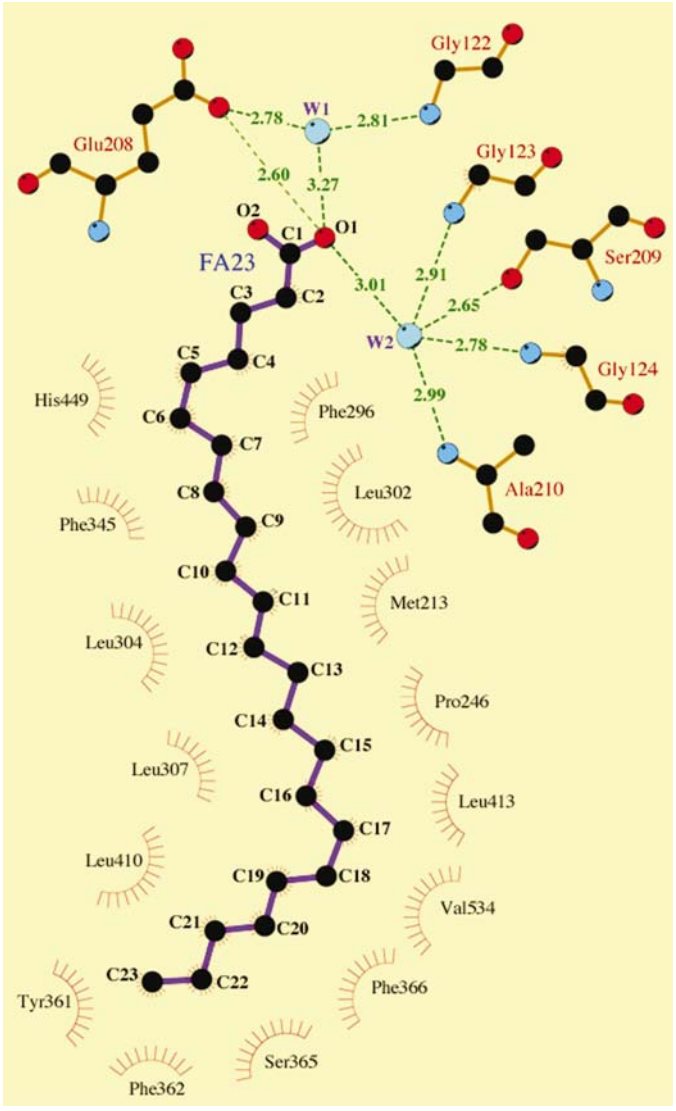

Figure 3
Illustration of amino-acid contacts to the proposed fatty-acid ligand ($C_{23}H_{48}O_2$) in the active-site gorge. Hydrogen bonds are shown as green dashed lines, waters as blue spheres and van der Waals contacts as bent red combs. Figure produced using *LIGPLOT*/*HBPLUS* (Wallace *et al.*, 1995; McDonald & Thornton, 1994).

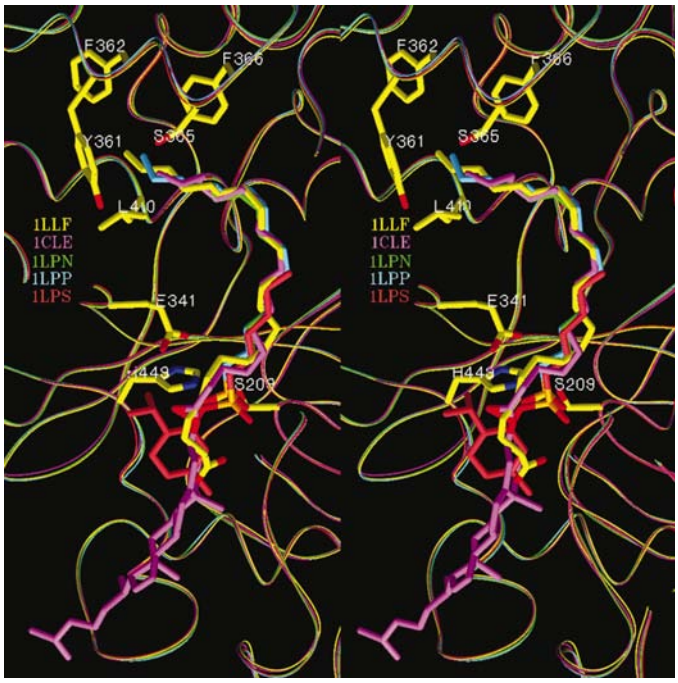

Figure 4
Stereoview of the least-squares superimposed ligand-bound structures: *C. cylindracea* cholesterol esterase (ChE) complexed with fatty acid $C_{23}H_{48}O_2$ (FA23) (PDB code 1llf; yellow) and with cholesteryl linoleate (PDB code 1cle; magenta) and *C. rugosa* lipase complexed with dodecanesulfonate ($C_{12}H_{26}SO_2$; PDB code 1lpn; green), hexadecanesulfonate ($C_{16}H_{34}SO_2$; 1lpp; blue) and menthyl hexyl phosphonate ($C_{16}H_{32}PO_2$; 1lps; orange). The enzyme catalytic triad residues Ser209, Glu341, His449 and the residues Tyr361, Phe362, Ser365, Phe366, Leu410 at the bottom of the tunnel are shown. Figure produced with *SETOR* (Evans, 1993).

conformation of the FA23 differs significantly from the tetrahedral intermediate state conformation of the HDS that is covalently bound to Ser209. At the reactive site the position of the C5 atom of FA23 is similar to the position of the carbonyl C atom in the substrate. It is ~3.5 Å apart from the O^{γ} atom of the catalytic Ser209, compared with the corresponding ~1.5 Å bonding distance between O^{γ} and the S atom of HDS in the lipase complex. This apparently causes the observed conformational difference in the ChE/lipase ligand sections preceding the structurally similar parts.

Relative to the linoleate and HDS ligands in their respective ChE and lipase complexes (Ghosh *et al.*, 1995; Grochulski *et al.*, 1994), the terminal C23 atom in the ChE–FA23 complex is buried 3.0 and 1.46 Å deeper in the tunnel, respectively. As a consequence, this atom resides in the deepest possible position, which is 3.65 Å from the residues Tyr361/1361 and Phe362/1362. Despite the fact that the ligands extend into the tunnel to different extents, in all three complexes compared the positions of the enzyme side chains at the bottom of the tunnel are nearly identical (except for the two terminal C^{δ} atoms of the Leu410 side chain).

This could indicate that depending on the saturation level C_{18}/C_{19}-chain fatty acids of cholesterol esters are of the maximum length suitable for productive binding for hydrolysis. The longer fatty acids sterically restrict the reactive-site occupation and are very likely to behave as competitive inhibitors.

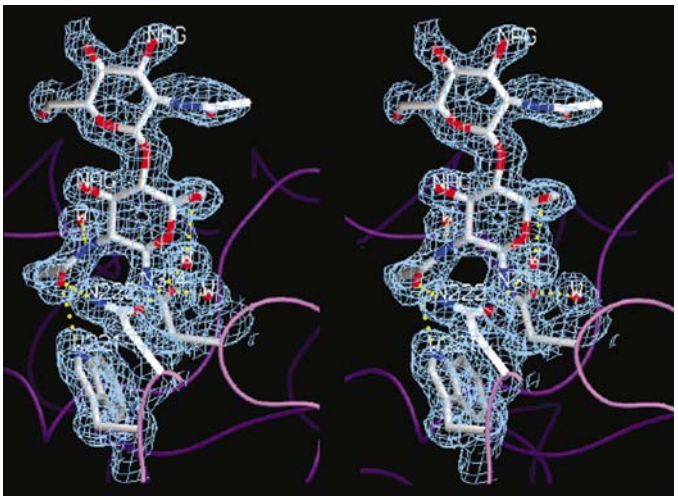

Figure 5
Stereoview of the two *N*-acetyl-D-glucosoamine moieties chain covalently bound to the Asn314 side chain in the $2F_o - F_c$ electron-density map (blue; contoured at $1.0\sigma_{\rho}$). Hydrogen bonds are indicated by yellow pointed lines, waters (W) by red spheres. Figure produced with *SETOR* (Evans, 1993).

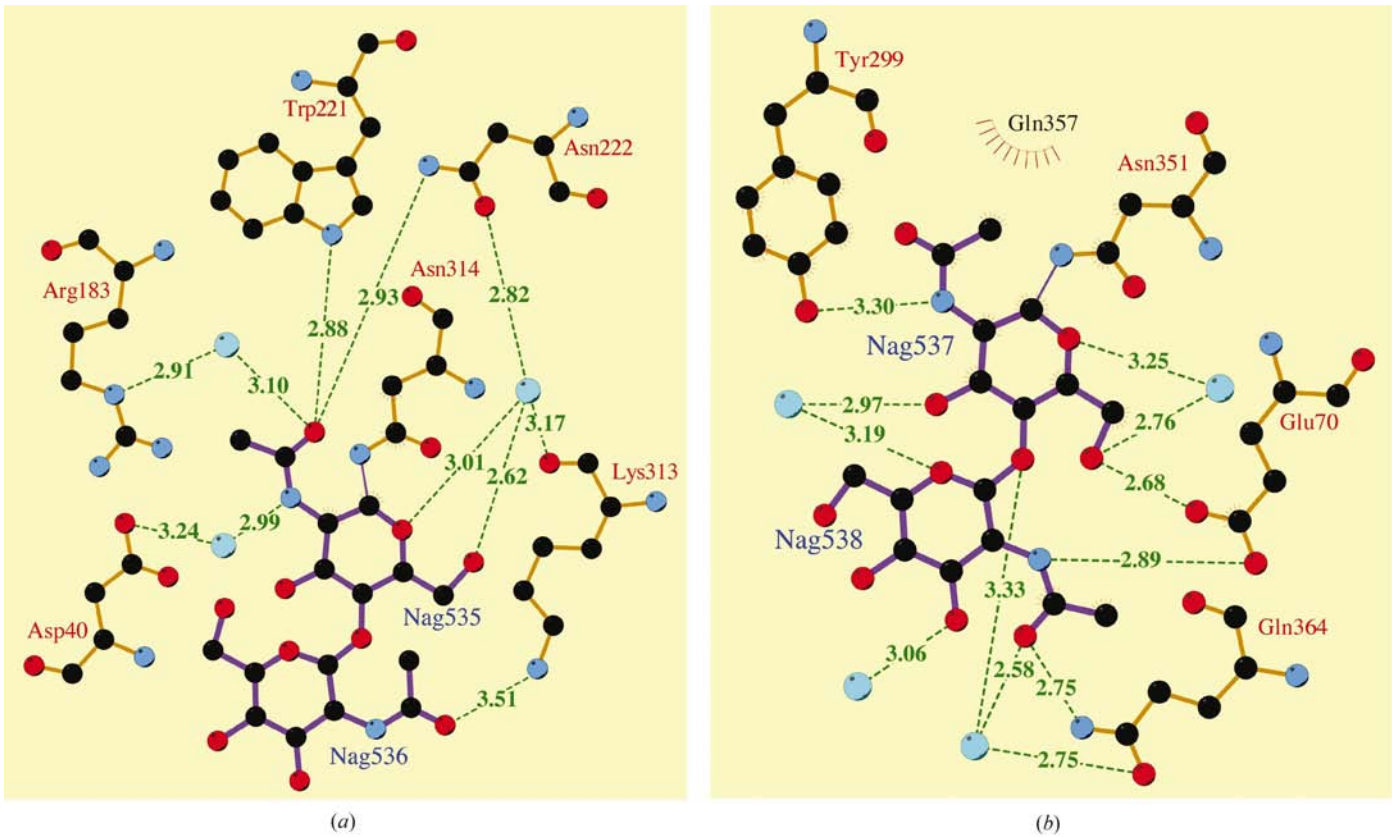

Figure 6
A scheme showing the enzyme stereochemical environment for the NAG carbohydrate chains at the Asn314 (*a*) and Asn351 (*b*) sites. Hydrogen bonds are shown by green dashed lines, waters by blue spheres and van der Waals contacts by bent red combs. Figure produced using *LIGPLOT*/*HBPLUS* (Wallace *et al.*, 1995; McDonald & Thornton, 1994).

3.3. Carbohydrate composition

In the ChE–linoleate and lipase–MPC/DSC/HDS structures (Ghosh *et al.*, 1995; Grochulski *et al.*, 1994) the observed positions of the *N*-acetyl-D-glucosoamine (NAG) moieties covalently bound to Asn314 and Asn351 side chains are nearly identical. The enzyme stereochemical shells and most of the essential bridging waters interacting with carbohydrates are very similar to those found for the ChE–FA23 complex. The exceptions are two mutations, K313V and F69Y, observed in lipase at the Asn314 and Asn351 sites, respectively, and resulting in an additional stabilizing hydrogen bond at the Asn351 site between the Tyr69 side chain and the terminal NAG moiety.

In contrast to these previously determined structures, the 1.4 Å resolution low-temperature data allowed us to unequivocally locate an additional carbohydrate moiety in the ChE–FA23 complex. This sugar moiety NAG536/1536 is attached to NAG535/1535, which is covalently bound to the Asn314/1314 side chain (Fig. 5). Each subunit has well defined electron density corresponding to two NAG molecules at each site, Asn314/1314 and Asn351/1351. Six of the eight NAG molecules in the dimer, 535/1535, 537/1537 and 538/1538, are stabilized by the extensive network of hydrogen bonds to the enzyme, which are either direct or mediated by waters (Fig. 6). The position of NAG536/1536 is stabilized by one relatively weak salt bridge (3.51 Å) between the carbohydrate *N*-acetyl group and the enzyme Lys313/1313 side chain in the new (compared with the ChE–linoleate complex) orientation. The lack of stabilization contacts for the terminal NAG536/1536 at the Asn314/1314 site is reflected by the weaker electron density.

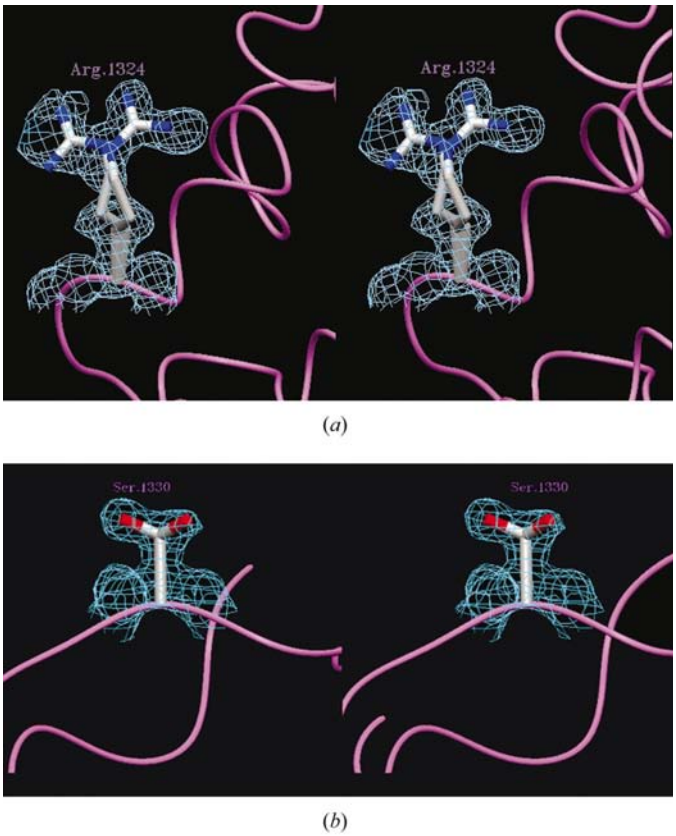

Figure 7
Stereoview of Arg1324 (*a*) and Ser1330 (*b*) illustrating the multiple side-chain conformations in the $2F_o - F_c$ electron density (blue; contoured at $1.1\sigma_\rho$). Figure produced with *SETOR* (Evans, 1993).

3.4. Dynamic features and corrections

Two alternative conformations with occupancy values of 0.5 ± 0.2 were detected for the side chains in 14 residues, including those of Val86, Ser201, Ser264, Arg324, Met445 and Ser496 in the first subunit and those of Val1086, Val1090, Ser1264, Ser1272, Leu1313, Arg1324, Ser1330 and Met1445 in the second subunit (Fig. 7).

The data also allowed us to identify unambiguously the correct amino acid at position 344/1344. The controversy between Val from the X-ray structure (PDB code 1cle; Ghosh *et al.*, 1995), Leu from the protein sequence (PIR accession No. S41735; Kaiser *et al.*, 1994) and Ile from the DNA sequence of the enzyme precursor (SWISS-PROT accession No. P32947; Lotti *et al.*, 1993) was resolved in favor of Ile.

3.5. Water structure

In addition to the 478 water molecules found previously (Ghosh *et al.*, 1995), 600 further water molecules were located using 1.4 Å resolution data. Approximately 50 waters were found in the intradimer hydrophobic cavity, principally near the edges of the four entry sites. In addition, well defined and conserved water molecules were located within hydrogen-bonding distance of the catalytic Ser209 side chain and the FA23 ligand (Figs. 5 and 6), within 4 Å of the catalytic Glu341 and His449 side chains, and at the active-site gorge exit.

This research was partly supported by the NIH grant 4 R37 DK26546-34. Part of this work was performed at the DuPont–Northwestern–Dow Collaborative Access Team (DND-CAT) Synchrotron Research Center located at Sector 5 of the Advanced Photon Source. DND-CAT is supported by E. I. DuPont de Nemours & Co., the Dow Chemical Company, the US National Science Foundation through grant DMR-9304725 and the State of Illinois through the Department of Commerce and the Board of Higher Education grant IBHE HECA NWU 96. Use of the Advanced Photon Source was supported by the US Department of Energy, Basic Energy Sciences, Office of Energy Research under Contract W-31-102-Eng-38.

References

Bergmeyer, H. U., Grassi, M. & Walter, H. E. (1983). *Methods of Enzymatic Analysis*, Vol. 2, edited by H. U. Bergmeyer, pp. 168–169. Weinheim, Germany: Verlag Chemie.

Bourne, Y., Taylor, P., Bougis, P. E. & Marchot, P. (1999). *J. Biol. Chem.* **274**, 2963–2970.

Brünger, A. T., Adams, P. D., Clore, G. M., DeLano, W. L., Gros, P., Grosse-Kunstleve, R. W., Jiang, J.-S., Kuszewski, J., Nilges, M., Pannu, N. S., Read, R. J., Rice, L. M., Simonson, T. & Warren, G. L. (1998). *Acta Cryst.* D**54**, 905–921.

Collaborative Computational Project, Number 4 (1994). *Acta Cryst.* D**50**, 760–763.
Cygler, M. & Schrag, J. D. (1999). *Biochim. Biophys. Acta*, **1441**, 205–214.
Cygler, M., Schrag, J. D., Sussman, J. L., Harel, M., Silman, I., Gentry, M. K. & Doctor, B. P. (1993). *Protein Sci.* **2**, 366–382.
Evans, S. V. (1993). *J. Mol. Graph.* **11**, 134–138.
Ghosh, D., Erman, M. & Duax, W. (1991). *J. Steroid Biochem. Mol. Biol.* **38**, 663–665.
Ghosh, D., Erman, M., Sawicki, M. W., Lala, P., Weeks, D. R., Li, N., Pangborn, W., Thiel, D. J., Jornvall, H. & Eyzaguirre, J. (1999). *Acta Cryst.* D**55**, 779–784.
Ghosh, D., Wawrzak, Z., Pletnev, V. Z., Li, N., Kaiser, R., Pangborn, W., Jornvall, H., Erman, M. & Duax, W. L. (1995). *Structure*, **3**, 279–288.
Grochulski, P., Bouthillier, F., Kazlauskas, R. J., Serreqi, A. N., Schrag, J. D., Ziomek, E. & Cygler, M. (1994). *Biochemistry*, **33**, 3494–3500.
Kaiser, R., Erman, M., Duax, W. L., Ghosh, D. & Jornvall, H. (1994). *FEBS Lett.* **337**, 123–127.
Kim, K. K., Song, H. K., Shin, D. H., Hwang, K. Y., Choe, S., Yoo, O. J. & Suh, S. W. (1997). *Structure*, **5**, 1571–1584.
Laskowski, R. A., MacArthur, M. W., Moss, D. S. & Thornton, J. M. (1993). *J. Appl. Cryst.* **26**, 283–291.
Lawson, D. M., Derewenda, U., Serre, L., Ferri, S., Szittner, R., Wei, Y., Meighen, E. A. & Derewenda, Z. S. (1994). *Biochemistry*, **33**, 9382–9388.
Lotti, M., Grandori, R., Fusetti, F., Longhi, S., Brocca, S., Tramonitano, A. & Alberghina, L. (1993). *Gene*, **124**, 45–55.
McDonald, I. K. & Thornton, J. M. (1994). *J. Mol. Biol.* **238**, 777–793.
Navaza, J. (1994). *Acta Cryst.* A**50**, 157–163.
Otwinowski, Z. & Minor, W. (1997). *Methods Enzymol.* **276**, 307–326.
Roeschlau, P., Bernt, E. & Gruber, W. (1974). *J. Clin. Chem. Clin. Biochem.* **12**, 403–407.
Sack, J. S. J. (1988). *J. Mol. Graph.* **6**, 224–225.
Sheldrick, G. (1997). *SHELXL*97. University of Göttingen, Germany.
Small, D. M. (1989). *Arteriosclerosis*, **8**, 103–129.
Sussman, J. S., Harel, M., Frolow, F., Oefner, C., Goldman, A., Toker, L. & Silman, I. (1991). *Science*, **253**, 872–879.
Uwajima, T. & Terada, O. (1975). *Agric. Biol. Chem.* **39**, 1511–1512.
Van Tilbeurgh, H., Egloff, M. P., Martinez, C., Rugani, N., Verger, R. & Cambillau, C. (1993). *Nature (London)*, **362**, 814–820.
Wallace, A. C., Laskowski, R. A. & Thornton, J. M. (1995). *Protein Eng.* **8**, 127–134.